Engineering Transactions, **71**(1): 111–140, 2023, doi: 10.24423/EngTrans.2460.20230214
Institute of Fundamental Technological Research Polish Academy of Sciences (IPPT PAN)
Université de Lorraine • Poznan University of Technology

Research Paper

On Spatial vs Referential Isotropic Fourier's Law in Finite Deformation Thermomechanics

Balbina WCISŁO[1)]*, Jerzy PAMIN[1)], Lars ROSE[2)], Andreas MENZEL[2),3)]

[1)] *Chair of Computational Engineering, Cracow University of Technology*
Cracow, Poland

[2)] *Institute of Mechanics, TU Dortmund University*
Dortmund, Germany

[3)] *Division of Solid Mechanics, Lund University*
Lund, Sweden

*Corresponding Author e-mail: balbina.wcislo@pk.edu.pl

This paper deals with the issue of isotropic heat conduction in thermomechanical large-strain problems. The aim of the paper is a comparison of different variants of Fourier's law used in the literature for a large strain problem. In particular, Fourier's law is specified either in the reference or in the deformed configuration by using different options of heat flux density vectors which are presented and discussed. The paper includes working examples to illustrate the presented theory. Moreover, different formulations of Fourier's law are tested by using the finite element method to investigate the influence of the applied variant on simulation results. The analysis reveals that in a strongly deformed area the temperature distribution varies.

Keywords: heat conduction; isotropic Fourier's law; large strains; thermomechanical coupling.

1. Introduction

Constitutive modelling of materials undergoing large deformations in non-isothermal conditions is an issue raised in numerous publications. A motivation for the development of such models can be the description of the material behaviour in various temperature ranges from extreme cases such as fire conditions or hot forming to moderate temperature increases due to elastic or plastic effects, for example, a Gough-Joule phenomenon or plasticity induced dissipation, respectively. Fully coupled models usually take into account the impact of temperature changes on the mechanical field by considering thermal expansion as well as temperature-dependent material model parameters.

The problem of thermomechanical coupling is discussed in numerous papers and books. Very often it is limited to geometrically linear problems, see, e.g., thermoelasticity in [17]. Models for large-strain thermoelasticity, which are often applied for the description of rubber or polymer materials, are presented, for instance, in [2, 7, 15]. In turn, thermoplasticity, used for i.a. metallic materials, is discussed in small-strain setting in [18] and for large strains in [4, 6, 20–22]. The majority of publications are restricted to an isotropic material and heat flux. This assumption is neglected in [9]. The aspects of the numerical implementation of heat transfer and thermomechanical coupling can be found in [8, 19].

If large deformations are taken into account, referential (undeformed, initial) and current (deformed) configurations are considered. For this kinematic assumption, the state of the material can be described by using referential or spatial quantities referring to either of the two configurations. This also applies to quantities related to the thermal field, such as the heat flux density vector.

The standard constitutive relation for the heat flux density vector is the well-known Fourier's law. For small-strain problems, the heat flux vector is then calculated as the product of a positive definite second-order conductivity tensor multiplied by the negative gradient of temperature. In the case of large strains, Fourier's law is similarly defined in the literature. However, it is not clear which heat flux density vector and configuration should be chosen for the definition of this constitutive relation.

The aim of this paper is to contribute to the current status and understanding of isotropic heat conduction for large-strain thermomechanical problems in order to show and directly compare the effect of different definitions of Fourier's law. In this regard, a comprehensive analysis of different measures for the heat flux density vector is performed. It should be mentioned that the interpretation of isotropic heat conduction is not uniquely handled in the literature. For the sake of simplicity, the main focus lies in formulations with one scalar conductivity parameter. The problem is analysed by using simple working examples as well as by numerically using the finite element method (FEM). Two types of materials, rubber and aluminium, undergoing large strains, are considered to show how the definition of the constitutive relation for the heat flux density vector influences the results. It is worth mentioning that the investigations presented in the paper apply to all types of gradient flow, e.g., diffusion processes.

This paper is laid out as follows. In Sec. 2, a concise outline of the kinematics for a large-strain problem is presented and the relations which are used in the subsequent derivations are recalled. In Sec. 3, the definitions of three measures of the heat flux density vectors are presented and discussed. Section 4 includes the definitions of Fourier's law defined in the reference and current configurations. Section 5 presents the energy balance equation incorporating different Fourier's laws. In Sec. 6, simple analytical calculations of the different heat flux density

measures are presented, and the graphical interpretation of the results is discussed. In Sec. 7, the results of numerical simulations of a selected test for the two selected materials are presented. The paper is completed with concluding remarks in Sec. 8.

The following notation for vector and tensor products is used in this contribution: $\mathbf{a} \cdot \mathbf{b}$ denotes the scalar product of two vectors (i.e., $\mathbf{a} \cdot \mathbf{b} = a_i b_i$ in Cartesian index notation) and $\mathbf{A}\mathbf{a}$ represents the product of second-order tensor $\mathbf{A}$ and vector $\mathbf{a}$ resulting in a vector (i.e., $(\mathbf{A}\mathbf{a})_i = A_{ij} a_j$ in Cartesian index notation).

2. Aspects of large strain kinematics

The basis of kinematic relations for large-strain description can be found in numerous references, for example, [3] or [25]. In this section, we focus on aspects relevant to subsequent derivations, e.g. – we show the map of area elements between configurations needed in order to express the relations between different measures of heat flux density.

We consider the motion of a deformable body in a three-dimensional space. Vector $\mathbf{X}$ denotes the position of a material particle in the reference (initial, undeformed) configuration, whereas vector $\mathbf{x}(\mathbf{X}, t)$ indicates the position of the particle in the deformed (current) configuration at time t.

The deformation gradient $\mathbf{F}$ and its determinant J are defined as

$$\mathbf{F} = \frac{\partial \mathbf{x}}{\partial \mathbf{X}}, \qquad J = \det(\mathbf{F}) > 0. \tag{2.1}$$

The transformation of the incremental vector $\mathrm{d}\mathbf{X}$ in the reference configuration into its counterpart in the current configuration $\mathrm{d}\mathbf{x}$ is therefore given by

$$\mathrm{d}\mathbf{x} = \mathbf{F}\,\mathrm{d}\mathbf{X}. \tag{2.2}$$

The relation between the volume element $\mathrm{d}V$ in the referential configuration and the volume element $\mathrm{d}v$ in the current configuration is given via the determinant of the deformation gradient

$$\mathrm{d}v = J\,\mathrm{d}V. \tag{2.3}$$

In the reference configuration, the element of area $\mathrm{d}A$ with unit normal $\mathbf{N}$ is considered, see Fig. 1a. The following definition is introduced

$$\mathrm{d}\mathbf{A} = \mathbf{N}\,\mathrm{d}A. \tag{2.4}$$

On the other hand, in the current configuration, the element of area $\mathrm{d}a$ with unit normal $\mathbf{n}$ is used, see Fig. 1b, so that we define the following vector:

$$\mathrm{d}\mathbf{a} = \mathbf{n}\,\mathrm{d}a. \tag{2.5}$$

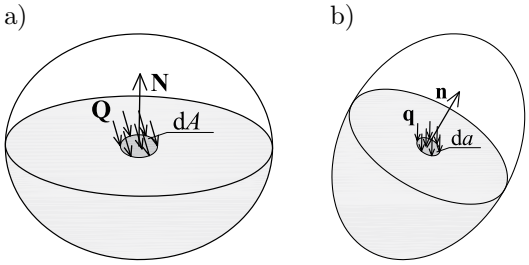

FIG. 1. Heat fluxes in reference (a) and current (b) configurations.

The transformation of the area element $\mathrm{d}\mathbf{A}$ to the current configuration, i.e., to the area element $\mathrm{d}\mathbf{a}$, is given by

$$\mathrm{d}\mathbf{a} = J\mathbf{F}^{-\mathrm{T}}\,\mathrm{d}\mathbf{A}. \tag{2.6}$$

The derivation of the above relation can be found in, e.g., [3].

The transformation of normal $\mathbf{N}$ in the reference configuration to normal $\mathbf{n}$ in the current one is given by the formula, see [1],

$$\mathbf{n} = \frac{\mathbf{F}^{-\mathrm{T}}\mathbf{N}}{|\mathbf{F}^{-\mathrm{T}}\mathbf{N}|}. \tag{2.7}$$

In the forthcoming derivations, we take into account material and spatial gradients of scalar quantities. Coefficients of the material gradient of a quantity G are calculated in the Cartesian basis as

$$\mathrm{Grad}(G) = \left[\frac{\partial G}{\partial X_1}, \frac{\partial G}{\partial X_2}, \frac{\partial G}{\partial X_3}\right]^{\mathrm{T}} \tag{2.8}$$

whereas coefficients of the spatial gradient of the quantity G in the Cartesian basis are

$$\mathrm{grad}(G) = \left[\frac{\partial G}{\partial x_1}, \frac{\partial G}{\partial x_2}, \frac{\partial G}{\partial x_3}\right]^{\mathrm{T}}. \tag{2.9}$$

The dependencies between the material and spatial gradients in absolute notation are as follows [25]:

$$\mathrm{Grad}(G) = \mathbf{F}^{\mathrm{T}}\,\mathrm{grad}(G), \tag{2.10}$$

$$\mathrm{grad}(G) = \mathbf{F}^{-\mathrm{T}}\,\mathrm{Grad}(G). \tag{2.11}$$

3. Transformation relations of heat flux densities

The aim of this section is the presentation and discussion of different measures for the heat flux density and the relations between them.

Vector $\mathbf{Q}$ denotes the Piola-Kirchhoff (or nominal) heat flux density vector in the reference configuration with the unit [W/m^2]. The amount of heat which flows through the area element $\mathrm{d}A$ (see Fig. 1) is therefore

$$-\mathbf{Q}\cdot\mathbf{N}\,\mathrm{d}A = -\mathbf{Q}\cdot\mathrm{d}\mathbf{A}, \tag{3.1}$$

with positive values indicating the inflow of heat.

On the other hand, vector $\mathbf{q}$ denotes the Cauchy heat flux density vector in the current configuration. The amount of heat which flows through an area element of the deformed configuration $\mathrm{d}a$ is calculated as

$$-\mathbf{q}\cdot\mathbf{n}\,\mathrm{d}a = -\mathbf{q}\cdot\,\mathrm{d}\mathbf{a} \tag{3.2}$$

The amount of heat flowing through the element area is the same in the reference and the current configuration; thus, the following equality can be written:

$$-\mathbf{Q}\cdot\,\mathrm{d}\mathbf{A} = -\mathbf{q}\cdot\,\mathrm{d}\mathbf{a}. \tag{3.3}$$

After inserting Eq. (2.6) into Eq. (3.2), the following dependence is obtained:

$$\mathbf{Q}\cdot\,\mathrm{d}\mathbf{A} = J\mathbf{q}\cdot(\mathbf{F}^{-\mathrm{T}}\,\mathrm{d}\mathbf{A}). \tag{3.4}$$

By using the algebraic relation $\mathbf{u}\cdot(\mathbf{S}\mathbf{v}) = \mathbf{v}\cdot(\mathbf{S}^{\mathrm{T}}\mathbf{u})$, the following transformations between the heat flux density vectors are obtained:

$$\mathbf{Q} = J\mathbf{F}^{-1}\mathbf{q}, \tag{3.5}$$

$$\mathbf{q} = J^{-1}\mathbf{F}\mathbf{Q}. \tag{3.6}$$

The above relations can be found, for example, in [6].

In addition to the Piola-Kirchhoff and the Cauchy heat flux density vectors, a third measure is often used in the literature called the Kirchhoff heat flux density vector, denoted here with $\widehat{\mathbf{q}}$. This vector is defined as the Cauchy heat flux density vector multiplied by the determinant of the deformation gradient

$$\widehat{\mathbf{q}} = J\mathbf{q}. \tag{3.7}$$

The following relations hold:

$$\mathbf{Q} = \mathbf{F}^{-1}\widehat{\mathbf{q}}, \tag{3.8}$$

$$\mathbf{q} = J^{-1}\widehat{\mathbf{q}}, \tag{3.9}$$

$$\widehat{\mathbf{q}} = J\mathbf{q} = \mathbf{F}\mathbf{Q}. \tag{3.10}$$

It is worth mentioning that the relations between different heat flux measures are sometimes not consistent in the literature. For example, the relation between the Kirchhoff and the Piola-Kirchhoff heat flux densities in [21] is given as $\widehat{\mathbf{q}} = \mathbf{F}^{-\mathrm{T}}\mathbf{Q}$, see the third line of Remark 56.1 in [21]. The relation from [21] resembles Eq. (2.11); however, it should be emphasised that Eq. (2.11) is valid for the gradients of a scalar quantity (which results in a vector), whereas $\mathbf{Q}$ and $\widehat{\mathbf{q}}$ are vector densities. In turn, in [4], the definitions of the heat flux measures are not clearly presented. The energy balance, i.e., Eq. (53) in [4], includes the divergence in the referential configuration $\mathrm{DIV}(\mathbf{F}^{-\mathrm{T}}\mathbf{q})$, where $\mathbf{q}$ is defined as the "heat flux vector" (most probably the Cauchy heat flux density vector), which is not consistent with the above transformations.

4. Fourier's law for large strain deformations

In this section, attention is paid to constitutive relations for the heat flux, in particular to Fourier's law. For the finite strain problem, the relation can be represented in the reference or the current configuration. In the former case, the relation is specified for the Piola-Kirchhoff heat flux density vector, whereas for the latter the Cauchy or Kirchhoff heat flux measures can be used. The way in which Fourier's law is written is a constitutive choice and all three variants can be found in the literature. The effect of this choice is investigated in this paper.

4.1. Fourier's law in the reference configuration

Fourier's law can be specified in the reference configuration for the Piola-Kirchhoff heat flux density vector in the following form:

$$\mathbf{Q} = -\mathbf{K}\,\mathrm{Grad}(T), \tag{4.1}$$

where $T = T(\mathbf{X}, t) > 0$ denotes the absolute temperature of particle $\mathbf{X}$ at time t. Tensor $\mathbf{K}$ represents conductivity, and for an isotropic heat conduction, it is assumed as

$$\mathbf{K} = K\mathbf{I}, \tag{4.2}$$

where K is a parameter specified for the analysed undeformed material and $\mathbf{I}$ is the second-order identity tensor. In general, K is assumed to be dependent on temperature, see [4]. However, in this work, it is considered constant. The unit of conductivity is $[\mathrm{J}/(\mathrm{s}\cdot\mathrm{m}\cdot\mathrm{K})]$ or equivalently $[\mathrm{N}/(\mathrm{s}\cdot\mathrm{K})]$. The conductivity parameter K cannot be transformed from the undeformed to the deformed configuration as easily as a parameter given per unit of volume, i.e., through scaling via the determinant of the deformation gradient.

The constitutive choice (4.1) can be found in the literature, for example, in [4]. The transformation of Eq. (4.1) to the current configuration using Eqs (2.10) and (3.5) yields

$$\mathbf{q} = -\frac{1}{J}\mathbf{F}\mathbf{K}\mathbf{F}^{\mathrm{T}}\,\mathrm{grad}(T). \tag{4.3}$$

Assuming that, in the reference configuration, the heat flux is isotropic, i.e., $\mathbf{K} = K\mathbf{I}$, the above equation can be rewritten as

$$\mathbf{q} = -\frac{1}{J}K\mathbf{b}\,\mathrm{grad}(T), \tag{4.4}$$

where $\mathbf{b} = \mathbf{F}\mathbf{F}^{\mathrm{T}}$ is the left Cauchy-Green deformation tensor. Equation (4.4) can be formulated in the following form:

$$\mathbf{q} = -\mathbf{k}(\mathbf{F})\,\mathrm{grad}(T), \tag{4.5}$$

where

$$\mathbf{k}(\mathbf{F}) = \frac{1}{J}K\mathbf{b}. \tag{4.6}$$

Equation (4.5) clearly shows that if isotropic Fourier's law is assumed in the reference configuration, then the Cauchy heat flux density vector is related to the spatial gradient of temperature via tensor $\mathbf{k}$ dependent on the deformation. As a result, the spatial heat flux density vector is non-parallel to the temperature gradient in the deformed body.

4.2. Fourier's law in the current configuration

Based on the same idea as in the previous subsection, i.e., that the heat flux density vector is related to the temperature gradient via conductivity, Fourier's law can be represented in the current configuration by using the Cauchy heat flux density vector, see [23],

$$\mathbf{q} = -\mathbf{k}\,\mathrm{grad}(T), \tag{4.7}$$

where $\mathbf{k}$ is the conductivity tensor for the spatial formulation. For isotropic heat conduction, it is assumed as

$$\mathbf{k} = k\mathbf{I}, \tag{4.8}$$

where k is a scalar conductivity parameter.

Postulating that Fourier's law holds in the deformed configuration according to Eq. (4.7), the obtained heat flux density vector can be pulled back to the reference configuration by using Eqs (2.11) and (3.6) to yield

$$\mathbf{Q} = -J\mathbf{F}^{-1}\mathbf{k}\mathbf{F}^{-\mathrm{T}}\,\mathrm{Grad}(T) \tag{4.9}$$

and for the isotropic heat conduction, i.e., Eq. (4.8), the above equation is as follows:

$$\mathbf{Q} = -Jk\mathbf{C}^{-1}\,\mathrm{Grad}(T), \tag{4.10}$$

where $\mathbf{C} = \mathbf{F}^{\mathrm{T}}\mathbf{F}$ is the right Cauchy-Green deformation tensor. Equation (4.10) can be written in the following form, see [23]:

$$\mathbf{Q} = -\mathbf{K}(\mathbf{F})\,\mathrm{Grad}(T), \tag{4.11}$$

where

$$\mathbf{K}(\mathbf{F}) = J\mathbf{F}^{-1}\mathbf{k}\mathbf{F}^{-\mathrm{T}}. \tag{4.12}$$

Another option of Fourier's law in the current configuration is the relation written for the Kirchhoff heat flux density vector

$$\widehat{\mathbf{q}} = -\mathbf{k}\,\mathrm{grad}(T). \tag{4.13}$$

This relation can be found in, e.g., [21, 22] or [26]. The same constant value of conductivity is usually used in the literature for Eqs (4.7) and (4.13), although the first equation is defined for the purely spatial heat flux density $\mathbf{q}$, whereas the second is stated for the heat flux density $\widehat{\mathbf{q}}$, which is scaled via the determinant of the deformation gradient. Moreover, often the scalar conductivity parameter is considered as a material property rather than being referred to as a referential or spatial form of Fourier's law.

If Eq. (4.13) is adopted, the corresponding Piola-Kirchhoff heat flux density vector is as follows:

$$\mathbf{Q} = -\mathbf{F}^{-1}\mathbf{k}\mathbf{F}^{-\mathrm{T}}\,\mathrm{Grad}(T) \tag{4.14}$$

and for the isotropic heat conduction it equals

$$\mathbf{Q} = -k\mathbf{C}^{-1}\,\mathrm{Grad}(T). \tag{4.15}$$

Fourier's law for the isotropic heat conduction defined in the current configuration is assumed in such a way that the Cauchy heat flux (or the Kirchhoff

heat flux) is proportional to the temperature gradient via a scalar value of conductivity in the deformed body; thus, $\mathbf{q}$ (or $\widehat{\mathbf{q}}$) is parallel to the spatial gradient of temperature. It can be understood that in this approach, the isotropy of the heat flux is considered in the current configuration. However, with this assumption, the Piola-Kirchhoff heat flux can be non-parallel to the temperature gradient in the reference configuration. In other words, in the reference configuration, the Piola-Kirchhoff heat flux is related to the material gradient of temperature through $\mathbf{K}$ that depends on the deformation gradient $\mathbf{F}$. In this situation, conductivity in the reference configuration cannot be reduced to a scalar value. Thus, in the reference configuration, the heat flux can then be treated as anisotropic. This observation is of great importance for a proper understanding of the heat flow for large strain problems.

To sum up this section, the most common constitutive equation for the heat flux used in thermomechanics, that is, the isotropic Fourier's law, is equivocal in the large strain context as it can be defined in the reference or spatial configuration. All choices are valid; however, from the physics point of view, the most reasonable is the approach where the spatial heat flux is parallel to the temperature gradient in the current configuration. For this variant one must be aware that the Piola-Kirchhoff heat flux density vector is not parallel to the temperature gradient in the material configuration. On the other hand, the deformation of an initially isotropic material can cause its anisotropy, for instance, the reorientation of polymer chains in rubber-like materials, which can justify the application of referential Fourier's law resulting in non-parallel Cauchy heat flux density vector and temperature gradient in the current configuration. However, the deformation-induced anisotropy of a material is not necessarily related to its thermal properties such as heat conductivity. In general, the particular format of the heat flux relation should be validated on the basis of experimental investigations. It is worth mentioning that the referential Fourier's law can be convenient for numerical implementation since it involves the material gradient of temperature.

A complete list summarising the three presented variants of isotropic Fourier's law and the resulting relations for the heat flux density measures are presented in Table 1.

Table 1. Heat fluxes for different isotropic Fourier's law variants.

Fourier's law	Piola-Kirchhoff heat flux	Cauchy heat flux	Kirchhoff heat flux
$\mathbf{Q} = -K\,\mathrm{Grad}(T)$	•	$\mathbf{q} = -J^{-1}K\mathbf{b}\,\mathrm{grad}(T)$	$\widehat{\mathbf{q}} = -K\mathbf{b}\,\mathrm{grad}(T)$
$\mathbf{q} = -k\,\mathrm{grad}(T)$	$\mathbf{Q} = -Jk\mathbf{C}^{-1}\,\mathrm{Grad}(T)$	•	$\widehat{\mathbf{q}} = -Jk\,\mathrm{grad}(T)$
$\widehat{\mathbf{q}} = -k\,\mathrm{grad}(T)$	$\mathbf{Q} = -k\mathbf{C}^{-1}\,\mathrm{Grad}(T)$	$\mathbf{q} = -J^{-1}k\,\mathrm{grad}(T)$	•

5. Heat fluxes in energy balance

The coupled thermomechanical problem is usually described by using two governing equations: the balance of linear momentum and the balance of energy. The former equation is well-described in the literature, see, e.g., [3] or [13]. In this section, only the latter one is presented with special attention paid to the conductive term in the view of different formulations of Fourier's law.

Here the energy balance equation in the temperature form, which is a convenient formulation for numerical implementation, is written following Eq. (57.15) from [21]

$$c_0\dot{T} = -\mathcal{H}_{\text{cond}} + \mathcal{R} + \mathcal{D}_{\text{mech}} - \mathcal{H}_{\text{thel}}, \tag{5.1}$$

where $\dot{T}$ is the temperature rate. All components of the above equation are expressed per unit of the reference volume: c_0 – the heat capacity, $\mathcal{H}_{\text{cond}}$ – conduction energy, $\mathcal{R}$ – external heat source, $\mathcal{D}_{\text{mech}}$ – mechanical dissipation and $\mathcal{H}_{\text{thel}}$ – thermoelastic energy related to the Gough-Joule effect. The conductive component $\mathcal{H}_{\text{cond}}$ can be written in terms of a chosen heat flux density measure. In particular, for the Piola-Kirchhoff heat flux it is equal to

$$\mathcal{H}_{\text{cond}} = \text{Div}(\mathbf{Q}). \tag{5.2}$$

The conductive term can also be expressed by using spatial heat flux measures, see [22],

$$\mathcal{H}_{\text{cond}} = J\,\text{div}(\mathbf{q}) = J\,\text{div}(\widehat{\mathbf{q}}/J). \tag{5.3}$$

In the above equations, the divergence of the Piola-Kirchhoff heat flux $\text{Div}(\mathbf{Q})$ is calculated with respect to material coordinates, whereas divergences $\text{div}(\mathbf{q})$ and $\text{div}(\widehat{\mathbf{q}})$ are computed with respect to spatial coordinates. Equation (5.1) is completed with proper boundary conditions for the temperature and the normal heat flux

$$\begin{aligned} T &= \overline{T} \quad \text{on} \quad \partial\Omega_0^T, \\ Q_N = -\mathbf{Q}\cdot\mathbf{N} &= \overline{Q} \quad \text{on} \quad \partial\Omega_0^Q, \end{aligned} \tag{5.4}$$

where $\partial\Omega_0 = \partial\Omega_0^T \cup \partial\Omega_0^Q$ is the boundary of the reference domain Ω_0 and $\partial\Omega_0^T \cap \partial\Omega_0^Q = \emptyset$. Moreover, the initial temperature condition must be specified.

The subsequent section of this paper presents the results of numerical simulations obtained with the finite element method (FEM). The method is based on a weak formulation of the initial boundary value problem. The weak form of Eq. (5.1) with the conductive term (5.3), boundary conditions (5.4), and with

Euler backward integration of $\dot{T}$ (T_n is the temperature from the previous time step and Δt is the time increment) is as follows:

$$\int_{\Omega_0} \delta T c_0 \frac{T - T_n}{\Delta t} \,\mathrm{d}V - \underbrace{\int_{\Omega_0} \mathrm{Grad}(\delta T) \cdot \mathbf{Q} \,\mathrm{d}V}_{\mathcal{I}_{\mathrm{cond}}} - \int_{\Omega_0} \delta T \left[\mathcal{R} + \mathcal{D}_{\mathrm{mech}} - \mathcal{H}_{\mathrm{thel}}\right] \mathrm{d}V - \int_{\partial\Omega_0^Q} \delta T \overline{Q} \,\mathrm{d}A = 0, \tag{5.5}$$

where δT is a test function, and the integration is performed over the reference domain, which in certain instances can be a more efficient approach from the computational point of view.

Now Fourier's law will be applied in the alternative forms presented in Eqs (4.1), (4.7) or (4.13). Inserting Fourier's law specified in the reference configuration in the form (4.1) with isotropy assumed, the following integral related to the conductive term in the weak form is obtained:

$$\mathcal{I}_{\mathrm{cond}} = -\int_{\Omega_0} \mathrm{Grad}(\delta T) \cdot k \,\mathrm{Grad}(T) \,\mathrm{d}V. \tag{5.6}$$

Using isotropic Fourier's law for the Cauchy heat flux density vector in the form (4.7) with the pull back from Eq. (4.10), the integral related to heat conduction is equal to

$$\mathcal{I}_{\mathrm{cond}} = -\int_{\Omega_0} \mathrm{Grad}(\delta T) \cdot Jk\mathbf{C}^{-1}\mathrm{Grad}(T) \,\mathrm{d}V \tag{5.7}$$

and for isotropic Fourier's law related to the Kirchhoff heat flux (4.13) with the relation from Eq. (4.15) the integral is as follows:

$$\mathcal{I}_{\mathrm{cond}} = -\int_{\Omega_0} \mathrm{Grad}(\delta T) \cdot k\mathbf{C}^{-1} \,\mathrm{Grad}(T) \,\mathrm{d}V. \tag{5.8}$$

6. Analytical example

To illustrate the influence of the deformation on the heat flux density vectors, we consider a simple 2D working example (plane strain) based on an exercise from [3] and enhanced with thermal coupling. Two aspects are analysed in this section. Firstly, the influence of the adopted Fourier's law formulation on heat

flux measures is investigated. Secondly, it is shown how the different measures of heat flux can be applied for the calculation of a resultant heat flux across a chosen boundary of the analysed specimen.

We consider a square section of the uniformly deformed material. The following mapping is given:

$$x_1 = \frac{1}{4}(18 + 4X_1 + 6X_2), \qquad x_2 = \frac{1}{4}(14 + 6X_2). \tag{6.1}$$

The initial and deformed configurations are presented in Fig. 2.

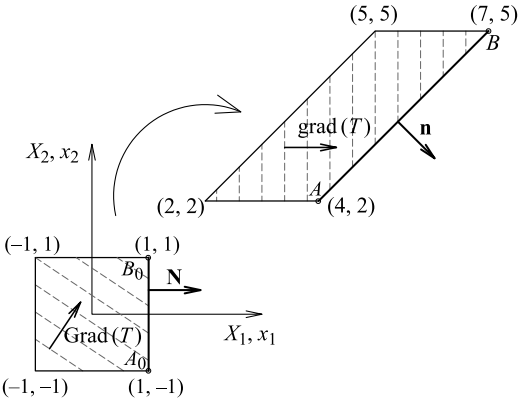

FIG. 2. Initial and deformed 2D specimen with isotherms (displacement and temperature field are fully prescribed).

The coefficients of the deformation gradient (reduced to 2D representation), its inverse and the determinant are as follows:

$$\mathbf{F} = \begin{bmatrix} \dfrac{\partial x_1}{\partial X_1} & \dfrac{\partial x_1}{\partial X_2} \\ \dfrac{\partial x_2}{\partial X_1} & \dfrac{\partial x_2}{\partial X_2} \end{bmatrix} = \frac{1}{2}\begin{bmatrix} 2 & 3 \\ 0 & 3 \end{bmatrix}, \qquad \mathbf{F}^{-1} = \frac{1}{3}\begin{bmatrix} 3 & -3 \\ 0 & 2 \end{bmatrix}, \qquad J = \frac{3}{2}. \tag{6.2}$$

The right and the left Cauchy-Green deformation tensors have the following coefficients:

$$\mathbf{C} = \mathbf{F}^{\mathrm{T}}\mathbf{F} = \frac{1}{2}\begin{bmatrix} 2 & 3 \\ 3 & 9 \end{bmatrix}, \qquad \mathbf{b} = \mathbf{F}\mathbf{F}^{\mathrm{T}} = \frac{1}{4}\begin{bmatrix} 13 & 9 \\ 9 & 9 \end{bmatrix}. \tag{6.3}$$

Let us assume that the temperature distribution in the current and the reference configuration is described with the functions

$$T(\mathbf{X}) = \frac{1}{4}(18 + 4X_1 + 6X_2)\xi, \qquad T(\mathbf{x}) = x_1\xi. \tag{6.4}$$

Parameter ξ is introduced to obtain appropriate units and has value 1. The material and the spatial gradients of the temperature field are constant vectors in the analysed domain and they are respectively equal to

$$\text{(6.5)} \qquad \operatorname{Grad}(T) = \begin{bmatrix} \dfrac{\partial T}{\partial X_1} \\ \dfrac{\partial T}{\partial X_2} \end{bmatrix} = \xi \begin{bmatrix} 1 \\ \dfrac{3}{2} \end{bmatrix}, \qquad \operatorname{grad}(T) = \begin{bmatrix} \dfrac{\partial T}{\partial x_1} \\ \dfrac{\partial T}{\partial x_2} \end{bmatrix} = \xi \begin{bmatrix} 1 \\ 0 \end{bmatrix}.$$

6.1. Heat fluxes for different variants of Fourier's law

6.1.1. Fourier's law in the reference configuration. Let us assume that isotropic Fourier's law is specified in the reference configuration for the Piola-Kirchhoff heat flux density vector, see Eq. (4.1). Using Eqs (3.9) and (3.10) the Cauchy and the Kirchhoff heat fluxes are then equal to

$$\text{(6.6)} \qquad \begin{gathered} \mathbf{Q} = -K \operatorname{Grad}(T) = -K\xi \begin{bmatrix} 1 \\ \dfrac{3}{2} \end{bmatrix}, \\ \mathbf{q} = -\frac{1}{6} K\xi \begin{bmatrix} 13 \\ 9 \end{bmatrix}, \qquad \widehat{\mathbf{q}} = -\frac{1}{4} K\xi \begin{bmatrix} 13 \\ 9 \end{bmatrix}. \end{gathered}$$

By using Eq. (4.4) the Cauchy heat flux can be represented in the following form:

$$\text{(6.7)} \qquad \mathbf{q} = -\frac{1}{J} K\mathbf{b} \operatorname{grad}(T) = -\begin{bmatrix} \dfrac{13}{6}K & \dfrac{3}{2}K \\ \dfrac{3}{2}K & \dfrac{3}{2}K \end{bmatrix} \operatorname{grad}(T) = -\frac{1}{6} K\xi \begin{bmatrix} 13 \\ 9 \end{bmatrix}.$$

Thus, conductivity in the current configuration is the tensor multiplying the spatial temperature gradient in Eq. (6.7).

It can be observed in this example that the Cauchy heat flux density vector $\mathbf{q}$ is not parallel to $\operatorname{grad}(T)$, see Fig. 3 (left).

6.1.2. Fourier's law in the current configuration Now the isotropic constitutive law for the heat flux is assumed in the current configuration, see Eq. (4.7). Then the Piola-Kirchhoff and the Kirchhoff heat fluxes are calculated by using Eqs (3.8) and (3.10) and are equal to

$$\text{(6.8)} \qquad \mathbf{q} = -k \operatorname{grad}(T) = -k\xi \begin{bmatrix} 1 \\ 0 \end{bmatrix}, \quad \mathbf{Q} = -k\xi \begin{bmatrix} \dfrac{3}{2} \\ 0 \end{bmatrix}, \quad \widehat{\mathbf{q}} = -k\xi \begin{bmatrix} \dfrac{3}{2} \\ 0 \end{bmatrix}.$$

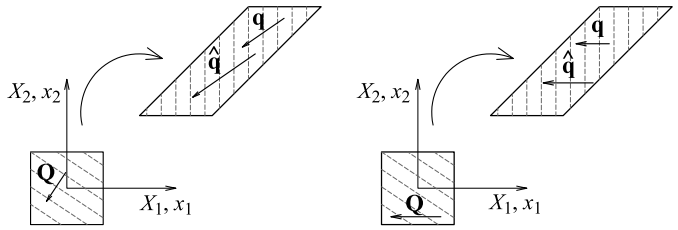

FIG. 3. Heat fluxes for Fourier's law defined in the reference configuration (left) and in the current configuration (right).

By analogy with Eq. (6.7), the Cauchy heat flux for Fourier's law defined in the reference configuration can be represented in the following form:

$$\mathbf{Q} = -Jk\mathbf{C}^{-1}\,\mathrm{Grad}(T) = -\begin{bmatrix} 3k & -k \\ -k & \dfrac{2}{3}k \end{bmatrix}\mathrm{Grad}(T) = -k\xi\begin{bmatrix} \dfrac{3}{2} \\ 0 \end{bmatrix}, \tag{6.9}$$

and conductivity in the reference configuration is the tensor multiplying the referential temperature gradient in Eq. (6.9).

In this case, it can be observed that the Piola-Kirchhoff heat flux density vector $\mathbf{Q}$ is not parallel to $\mathrm{Grad}(T)$, see Fig. 3 (right).

6.2. Heat fluxes across the surface

We focus on the heat flux through edge $A_0 - B_0$ in the reference configuration or its mapping $A - B$ in the current configuration, see Fig. 2. The unit vector normal to edge $A_0 - B_0$ is denoted by $\mathbf{N}$. The unit vector normal to edge $A - B$ is denoted by $\mathbf{n}$ and calculated via Eq. (2.7). They are respectively equal to

$$\mathbf{N} = \begin{bmatrix} 1 \\ 0 \end{bmatrix}, \qquad \mathbf{n} = \frac{\mathbf{F}^{-\mathrm{T}}\mathbf{N}}{|\mathbf{F}^{-\mathrm{T}}\mathbf{N}|} = \begin{bmatrix} \dfrac{\sqrt{2}}{2} \\ -\dfrac{\sqrt{2}}{2} \end{bmatrix}. \tag{6.10}$$

The length of edge $A_0 - B_0$ is equal to $|A_0B_0| = 2l_0$, where l_0 is a parameter introduced to obtain appropriate units, which has the value 1. The length of edge $A - B$ is thus $|AB| = 3\sqrt{2}l_0$. The depth of the specimen is denoted by d_0 in the following.

6.2.1. Fourier's law in the reference configuration. First, the analysis is performed for the heat flux density vectors from Eq. (6.6), i.e., for Fourier's law in the reference configuration. The amount of heat flowing through edge $A_0 - B_0$,

calculated by using the Piola-Kirchhoff heat flux density vector in the reference configuration, equals

$$\int\limits_{A_0-B_0} -\mathbf{Q}\cdot\mathbf{N}d_0\,\mathrm{d}S = -\mathbf{Q}\cdot\mathbf{N}d_0|A_0B_0| = 2K\xi d_0 l_0. \tag{6.11}$$

The amount of heat flowing through edge $A-B$ calculated in the current configuration using the Cauchy heat flux density vector is as follows

$$\int\limits_{A-B} -\mathbf{q}\cdot\mathbf{n}d_0\,\mathrm{d}s = -\mathbf{q}\cdot\mathbf{n}d_0|AB| = 2K\xi d_0 l_0. \tag{6.12}$$

Now the amount of heat is computed by using the Kirchhoff heat flux density vector. We derive the proper integration formula starting from the first part of Eq. (6.11)

$$\begin{aligned}\int\limits_{A_0-B_0} -\mathbf{Q}\cdot\mathbf{N}d_0\,\mathrm{d}S &= \int\limits_{A_0-B_0} -(\mathbf{F}^{-1}\widehat{\mathbf{q}})\cdot\mathbf{N}d_0\,\mathrm{d}S \\ &= \int\limits_{A_0-B_0} -\widehat{\mathbf{q}}\cdot(\mathbf{F}^{-\mathrm{T}}\mathbf{N})d_0\,\mathrm{d}S \neq \int\limits_{A_0-B_0} -\widehat{\mathbf{q}}\cdot\mathbf{n}d_0\,\mathrm{d}S.\end{aligned} \tag{6.13}$$

When the Kirchhoff heat flux density vector is used for integration, it is not multiplied by the unit normal $\mathbf{n}$ from the current configuration, but by a vector $\mathbf{F}^{-\mathrm{T}}\mathbf{N}$ which has the same direction as $\mathbf{n}$ and which is not normalized. Thus, the resultant heat is in this case equal to

$$\int\limits_{A_0-B_0} -\widehat{\mathbf{q}}\cdot(\mathbf{F}^{-\mathrm{T}}\mathbf{N})d_0\,\mathrm{d}S = -\widehat{\mathbf{q}}\cdot(\mathbf{F}^{-\mathrm{T}}\mathbf{N})d_0|A_0B_0| = 2K\xi d_0 l_0. \tag{6.14}$$

6.2.2. Fourier's law in the current configuration. The heat flux density vectors are now taken from Eq. (6.8), i.e., for Fourier's law in the current configuration. The amount of heat flowing through edge $A_0 - B_0$ calculated in the reference configuration by using the Piola-Kirchhoff heat flux density vector is as follows:

$$\int\limits_{A_0-B_0} -\mathbf{Q}\cdot\mathbf{N}d_0\,\mathrm{d}S = -\mathbf{Q}\cdot\mathbf{N}d_0|A_0B_0| = 3k\xi d_0 l_0. \tag{6.15}$$

The same calculations can be performed in the spatial configuration by using the Cauchy heat flux density vector

$$\int\limits_{A-B} -\mathbf{q}\cdot\mathbf{n}d_0\,\mathrm{d}s = -\mathbf{q}\cdot\mathbf{n}d_0|AB| = 3k\xi d_0 l_0. \tag{6.16}$$

Finally, the Kirchhoff heat flux density vector is applied for the calculations

$$\int_{A_0-B_0} -\widehat{\mathbf{q}} \cdot (\mathbf{F}^{-\mathrm{T}}\mathbf{N}) d_0 \, \mathrm{d}S = -\widehat{\mathbf{q}} \cdot (\mathbf{F}^{-\mathrm{T}}\mathbf{N}) d_0 |A_0 B_0| = 3k\xi d_0 l_0. \tag{6.17}$$

The results obtained for the different heat flux measures coincide as expected. If conductivity is considered as a material parameter independent of the deformation (i.e., values of K and k are the same), as it is usually assumed in the literature, then for the referential and spatial variants of Fourier's law, the amount of heat flowing through an analysed surface can vary significantly.

7. Numerical simulations

In this section, numerical simulations are performed in order to discuss the influence of the applied Fourier's law. The analysed specimen is an elongated rectangular plate with the dimensions $200 \times 100 \times 10$ mm, as presented in Fig. 4.

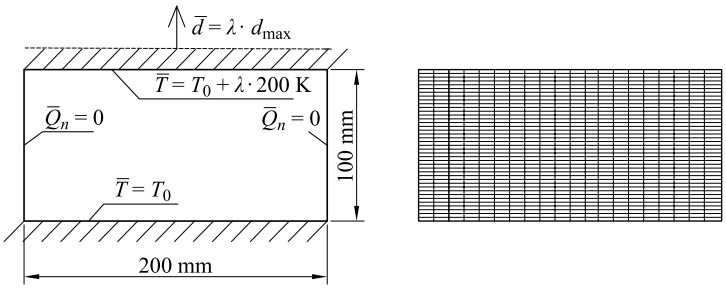

Fig. 4. Analysed plate in plane strain: boundary conditions, dimensions (left), and finite element discretisation with $20 \times 40 \times 1$ elements (right).

Plane strain conditions are assumed for the 3D configuration and the bottom surface is fully clamped. At the top side of the sample an enforced vertical displacement is applied, whereas the horizontal movement is constrained. Regarding the boundary conditions for the thermal field, the side walls are insulated, the bottom surface has constant temperature $T_0 = 293.15$ K, which corresponds to the initial temperature, and the prescribed temperature on the top surface of the sample increases together with deformation.

In the beginning, the vertical displacement and temperature in the essential boundary conditions on the top edge increase uniformly to $d_{\max}$ and $T_0 + 200$ K, respectively. In the second part of the process, the boundary conditions are fixed and heat flows in the specimen in order to obtain a stationary state. Figure 5 shows how multiplier λ in the essential boundary conditions depends on time for the deformation process duration time t_{proc}.

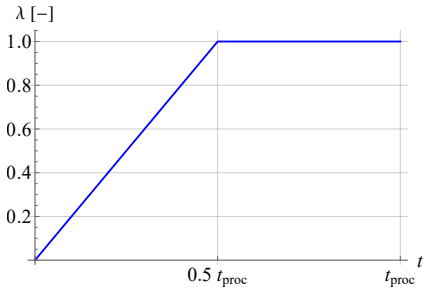

FIG. 5. Load multiplier vs time.

The simulations are performed for two different materials. The first is a natural rubber and the second is an aluminium alloy. The maximum value of the enforced displacement $d_{\max}$ is equal to 200 mm for rubber and 100 mm for aluminium.

The three possibilities to apply Fourier's law are considered:

- material Fourier's law for the Piola-Kirchhoff heat flux $\mathbf{Q} = -k\,\mathrm{Grad}(T)$ (variant 1),
- spatial Fourier's law for the Cauchy heat flux $\mathbf{q} = -k\,\mathrm{grad}(T)$ (variant 2),
- spatial Fourier's law for the Kirchhoff heat flux $\widehat{\mathbf{q}} = -k\,\mathrm{grad}(T)$ (variant 3).

The specimen is discretised using hexahedral elements with linear interpolation of displacement and temperature fields, here specified as H1 (the 2D problem is solved by using 3D elements). The primary mesh division is $20 \times 40 \times 1$ in the horizontal, vertical and thickness directions, respectively. To avoid volumetric locking for nearly incompressible rubber and for aluminium modelled within an isochoric plasticity framework, the modification of the finite elements called *F-bar* is applied [5]. An alternative approach based on the enhanced assumed strain approach can be found, for example, in [12].

Simulations have also been carried out for finite elements with quadratic interpolation of the displacement field and linear interpolation of temperature (elements H2/H1), in particular for rubber and the first variant of Fourier's law. In that case, the results for elements H2/H1 coincide with those obtained for elements H1 with *F-bar*.

All numerical tests are performed with *Wolfram Mathematica* packages called *AceGen* and *AceFEM* [10, 11] with user-defined subroutines for the two applied materials. An implementation of a thermoplastic model is presented, for instance, in [24]. The simulations are performed by using adaptive increments of time. The minimum and maximum increments are $0.001t_{\text{proc}}$ and $0.01t_{\text{proc}}$, respectively.

The energy balance equation is implemented via the weak form presented in Eq. (5.5) with the conductive term from Eqs (5.6), (5.7) or (5.8). We apply

the Euler backward integration scheme for the temperature rate in the energy balance equation, although different numerical time integration schemes could be used, see, e.g., [8].

7.1. Rubber

The thermomechanical coupling for rubber involves thermal expansion. For the sake of simplicity, thermoelastic coupling (Gough-Joule effect) is neglected in the energy balance. The adopted free energy function is as follows:

$$\psi(\mathbf{b},T)=\frac{1}{2}\kappa\left[\left[\ln(J^b)\right]^2-3\alpha_T[T-T_0]\ln J^b\right]+\frac{1}{2}\mu\left[[J^b]^{-1/3}\mathrm{tr}(\mathbf{b})-3\right], \tag{7.1}$$

where $J^b=\det(\mathbf{b})$ with $\mathbf{b}=\mathbf{F}\mathbf{F}^{\mathrm{T}}$, α_T is the linear coefficient of thermal expansion, and κ and μ are bulk and shear moduli, respectively. The material parameters used in simulations are based on [15] and presented in Table 2.

Table 2. Material parameters for rubber.

Property	Symbol	Value	Unit
Bulk modulus	κ	1950	$\mathrm{N/mm^2}$
Shear modulus	μ	0.4225	$\mathrm{N/mm^2}$
Thermal expansion coefficient	α_T	$6.36\cdot10^{-4}$	1/K
Conductivity	k	0.2	$\mathrm{N/(s\cdot K)}$
Heat capacity	c_0	1.5066	$\mathrm{N/(mm^2\cdot K)}$

In Fig. 6, the diagram presenting the total reaction force vs time is presented for process duration $t_{\mathrm{proc}}=600$ s. It can be observed that all curves in the left diagram almost coincide; however, a magnification of the middle part of the diagram reveals some differences in the total reaction force. The material response for variant 1 is softer than for variants 2 and 3 and the discrepancy grows with time in the second part of the simulated process. It seems that in this numerical test, the influence of the choice of Fourier's law on the global mechanical response is not significant. However, the mechanical response generally depends on the type of coupling (thermal softening, heat expansion), applied boundary conditions as well as on the values of model parameters.

The diagram in Fig. 7 (left) shows the sum of heat fluxes at nodes on the top side of the sample (called further the total "reaction" heat flux). It can be seen that all curves run in a similar way; however, the quantitative difference between them is significant. The amount of heat flowing through the analysed surface is the highest for variant 1. The difference between the results for variants 2 and 3 can be explained by the change of material volume caused by thermal

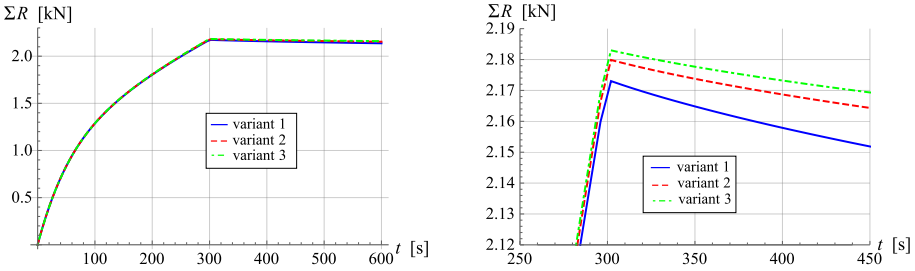

FIG. 6. Diagram of total reaction force vs time (left) and magnification of its middle part (right) for rubber sample.

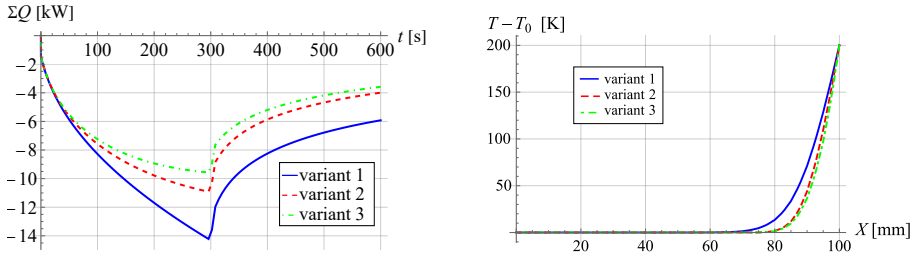

FIG. 7. Total "reaction" heat flux vs time (left) and final relative temperature distribution along the vertical central axis (right) for rubber sample.

expansion. The assumed Poisson ratio for rubber is equal to $\nu = 0.49$; thus, the change of material volume due to mechanical deformation is negligible.

The diagram in Fig. 7 (right) presents the relative temperature $T - T_0$ along the vertical central axis in the reference setting of the sample at the end of the simulated process. Due to the relatively small value of conductivity of rubber, only one-third of the sample undergoes heating. The boundary temperature is prescribed, but the temperature distribution in the internal part of the sample differs for the models with referential and spatial Fourier's laws. It can be observed that for variant 1, the temperature in the sample is higher than for variants 2 and 3, and the heated part of the sample is slightly wider.

The deformed meshes for variant 1 and variant 2 are depicted in Fig. 8. It can be observed that, due to small material conductivity, the temperature gradients are the largest in the upper part of the sample. The temperature considerably varies in the most deformed area and significant differences are visible in the top corners. For comparison, the temperature distribution in the undeformed mesh is also presented in Fig. 9. For variant 1, the isotherms are horizontal, whereas for variant 2, they are curved near the sides; thus, the influence of the deformation on the temperature distribution is visible in this area.

It can be noticed in the legends in Figs 8 and 9 (on the right) that the minimum relative temperature has a very small negative value. This is caused by

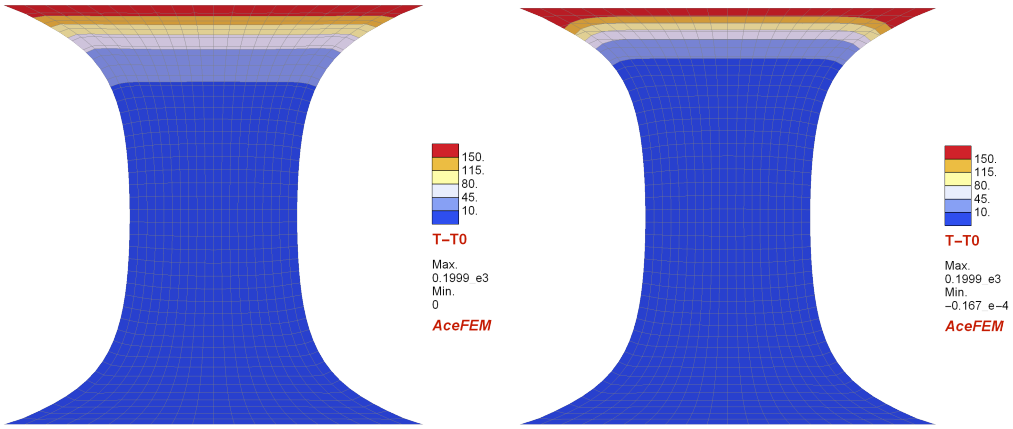

FIG. 8. Deformed mesh of rubber sample with relative temperature distribution at the end of simulation for variant 1 (left) and variant 2 (right) of Fourier's law.

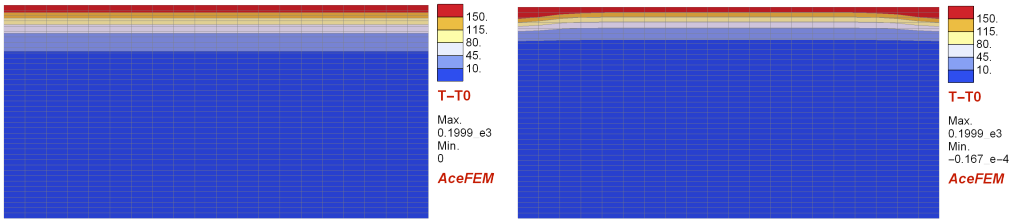

FIG. 9. Reference configuration of the rubber sample with final relative temperature distribution for variant 1 (left) and variant 2 (right) of Fourier's law.

small oscillations in temperature distribution in the lower part of the sample, which are caused by the applied time integration scheme, see [27]. The oscillations do not influence the results in the area of interest.

In Fig. 10, a magnification of the most deformed part of the sample is presented. In the centre of each finite element, the Cauchy heat flux density vector is visualised. It can be observed that for variant 1, vectors $\mathbf{q}$ are not perpendicular to isotherms and that directions are close to the directions of the Cauchy heat flux vectors for variant 2. However, the consistent scale of the displayed vectors shows that the magnitude of the heat flux is different for the two analysed cases.

To investigate the influence of the rate of the loading on the sample response the simulations are repeated for two and ten times longer processes, i.e., for $t_{\text{proc}} = 1200$ s and $t_{\text{proc}} = 6000$ s, which allows for the transport of more heat towards the centre of the specimen. For a faster process the influence of different Fourier's law expressions is smaller; thus, the case is not considered here. For all simulations, the increase of extension and temperature on the top surface lasts $0.5t_{\text{proc}}$. The results are presented in Figs 11 and 12.

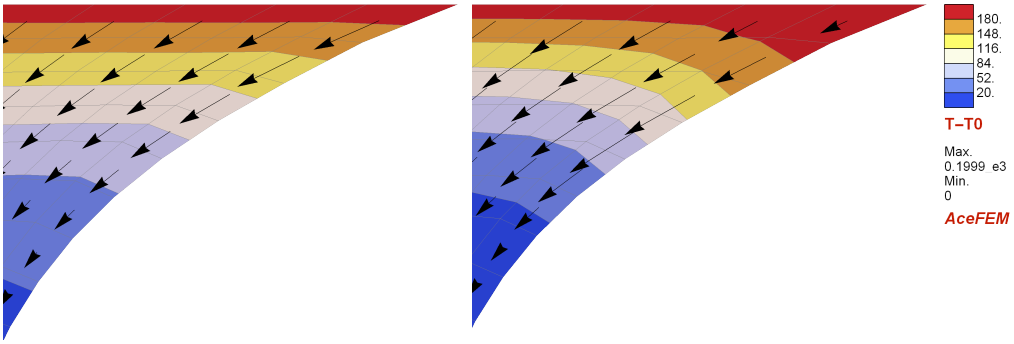

FIG. 10. Magnification of deformed mesh (right top corner of rubber sample) at the end of simulation with relative temperature distribution and Cauchy heat flux density vectors for variant 1 (left) and variant 2 (right) of Fourier's law.

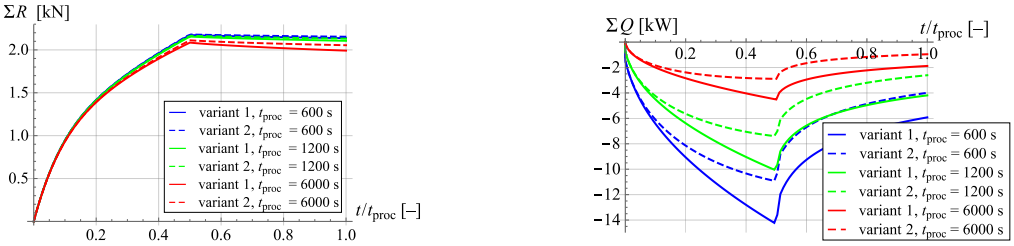

FIG. 11. Diagrams of total reaction force vs load multiplier (left) and of total "reaction" heat flux vs load multiplier (right) for rubber sample elongated with changing process duration.

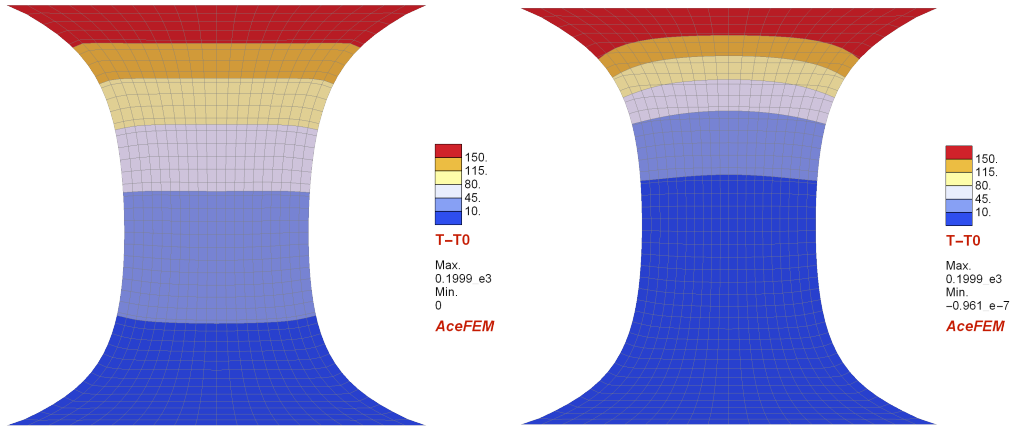

FIG. 12. Deformed mesh for rubber sample with relative temperature distribution at the end of simulation for variant 1 (left) and variant 2 (right) of Fourier's law and for slow process $t_{\mathrm{proc}} = 6000$ s.

It can be observed that the longer the process is, the more the curves of the reaction sum for the analysed variants of Fourier's law differ. However, the

differences are still very small. The application of variant 2 causes a slightly larger reaction force sum. In the case of the "reaction" heat flux sum, it can be seen that a longer process allows for a greater amount of heat flowing through the upper surface; however, for each process duration, the relations between curves obtained for variant 1 and variant 2 are similar. When the deformed sample is analysed, see Fig. 12, it can be seen that for variant 1 of Fourier's law a greater part of the sample is heated than for variant 2. When comparing this figure with the results obtained for $t_{\text{proc}} = 600$ s, see Fig. 8, it is observed that the influence of the applied Fourier's law has the same character. To sum up, for the analysed Fourier's law variants, the results obtained for changing process duration differ quantitatively but not qualitatively.

7.2. Aluminium

The second analysed material is aluminium alloy described with a thermoplastic material model that takes into account thermal expansion, plastic heating and thermal softening. In the model, the decomposition of the deformation gradient into reversible and plastic counterparts is applied, see [20], i.e.,

$$\mathbf{F} = \mathbf{F}^r \mathbf{F}^p. \tag{7.2}$$

The reversible part of the free energy function related to elastic deformation and thermal expansion is assumed in the following form:

$$\psi(\mathbf{b}^r, T) = \frac{1}{2}\kappa \left[\frac{1}{2}[J^{br} - 1] - \frac{1}{2}\ln(J^{br}) - 3\alpha_T[T - T_0]\ln(J^{br})\right] + \frac{1}{2}\mu\left[[J^{br}]^{-1/3}\,\mathrm{tr}(\mathbf{b}^r) - 3\right], \tag{7.3}$$

where $\mathbf{b}^r = \mathbf{F}^r\,[\mathbf{F}^r]^{\mathrm{T}}$ is the reversible left Cauchy-Green deformation tensor and $J^{br} = \det(\mathbf{b}^r)$.

The yield function F is introduced as

$$F(\boldsymbol{\tau}, \alpha, T) = f(\boldsymbol{\tau}) - \sigma_y(\alpha, T) \tag{7.4}$$

with

$$\sigma_y = \sqrt{\frac{2}{3}}\,[\sigma_{y0}\,[1 - H_T[T - T_0]] + [\sigma_{y\infty} - \sigma_{y0}]\,[1 - \exp(-\delta\alpha)]]. \tag{7.5}$$

The contribution $f(\boldsymbol{\tau})$ represents the Huber-Mises stress measure, here introduced for the Kirchhoff stress tensor $\boldsymbol{\tau} = 2[\partial\psi^r/\partial\mathbf{b}^r]\mathbf{b}^r$. Moreover, linear thermal softening with coefficient H_T and hardening of saturation type dependent

on hardening parameter α are accounted for. In the above equation, σ_{y0} and $\sigma_{y\infty}$ are the initial and the final yield strengths, respectively, and δ is a saturation constant.

The flow rule is written as

$$-\frac{1}{2}\mathcal{L}_v\mathbf{b}^r = \dot{\gamma}\mathbf{N}^p\mathbf{b}^r, \tag{7.6}$$

where $\mathcal{L}_v\mathbf{b}^r$ denotes the Lie derivative of the reversible left Cauchy-Green deformation tensor, see [13], $\mathbf{N}^p = \partial F/\partial\boldsymbol{\tau}$ is the normal to the yield function, and $\dot{\gamma}$ is the plastic multiplier.

The Kuhn-Tucker loading-unloading conditions complement the description

$$\dot{\gamma} \geq 0, \qquad F \leq 0, \qquad \dot{\gamma}F = 0. \tag{7.7}$$

The relation between the hardening parameter and the plastic multiplier is $\alpha = \sqrt{2/3}\gamma$.

The plastic heating contribution is considered via the simplified form, i.e., $\mathcal{D}_{\text{mech}} = \chi\dot{\alpha}\sigma_y$ where χ is the heat dissipation factor. The rate of hardening parameter $\dot{\alpha}$ is calculated in the code by using backward Euler integration, i.e., $\dot{\alpha} = [\alpha - \alpha_n]/\Delta t$, where α_n is the value of the hardening parameter from the previous time step.

Material parameters are taken from [16] and presented in Table 3.

Table 3. Material parameters for aluminium.

Property	Symbol	Value	Unit
Bulk modulus	κ	57 133	N/mm^2
Shear modulus	μ	26 369	N/mm^2
Initial yield strength	σ_{y0}	367.5	N/mm^2
Final yield strength	σ_{yf}	488.8	N/mm^2
Saturation constant	δ	16	N/mm^2
Conductivity	k	121	$\text{N/(s}\cdot\text{K)}$
Heat capacity	c_0	2.423	$\text{N/(mm}^2\cdot\text{K)}$
Thermal expansion coefficient	α_T	$23.2{\cdot}10^{-6}$	1/K
Thermal softening modulus	H_T	0.0016	1/K
Heat dissipation factor	χ	0.9	–

In Fig. 13, the diagrams of the total reaction force vs time are presented. In the left one, the results for the whole process are shown, and it can be seen that all curves are very close to each other. The diagram on the right presents a magnification of the middle part of the diagram on the left, where a slight difference in the sample response is visible. Similarly to the rubber specimen,

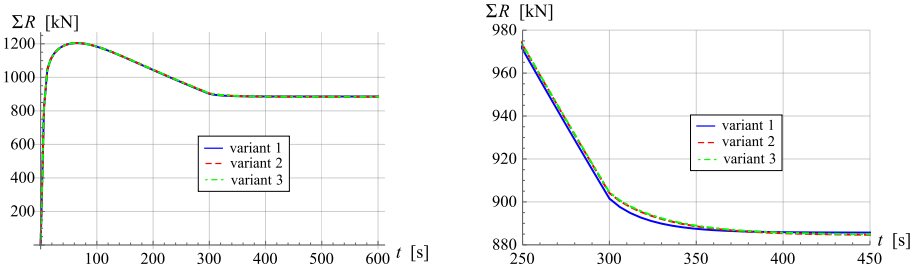

FIG. 13. Diagram of total reaction force vs time (left) and magnification of its middle part (right) for the aluminium sample.

the application of variant 1 of Fourier's law results in a slightly softer response of the material model.

The diagram in Fig. 14 (right) presents the amount of heat flowing through the upper surface vs time, which is much higher for variant 1 than for the other variants. The results for variants 2 and 3 are very close to each other. In this case, the prevailing type of deformation is plastic, which is isochoric for the Huber-Mises yield function. The final relative temperature distribution along the vertical central axis of the aluminium sample in the reference configuration is shown in Fig. 14 on the right. The application of variant 1 of Fourier's law results in a linear distribution of temperature along the sample, whereas spatial Fourier's laws cause a non-linear distribution.

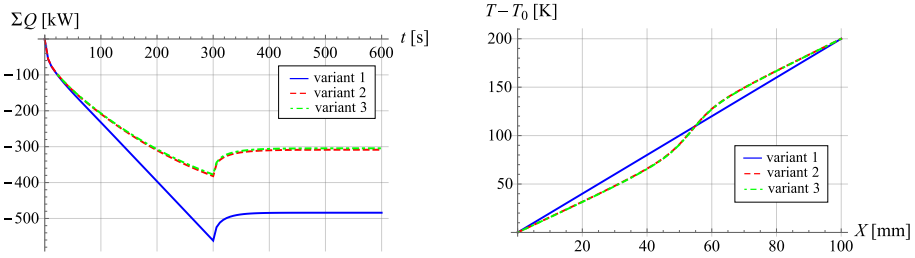

FIG. 14. Total "reaction" heat flux vs time (left) and relative temperature distribution along vertical central axis at the end of the simulation (right) for the aluminium sample.

In the analysed test, the aluminium sample undergoes softening caused by geometrical effects and thermal softening in the yield function, see Eqs (7.4) and (7.5). In the absence of regularisation, this could lead to strain localisation and pathological mesh dependence. In the analysed case, the regularising influence is provided only by heat conduction, see [14, 24]. To examine if the presented simulations are mesh-insensitive, we repeat calculations for variant 2 of Fourier's law using two and four times denser finite element meshes, see Fig. 15.

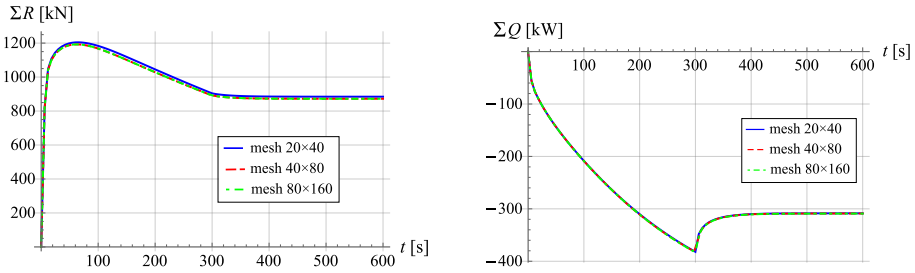

FIG. 15. Diagrams of total reaction force vs time (left) and of total "reaction" heat flux vs time (right) for the aluminium sample – comparison of results for different meshes.

The presented results confirm that heat conduction provides sufficient regularisation as the curves are very close for each discretisation.

The deformed primary meshes for variants 1 and 2 at the end of the deformation process are presented with temperature distributions in Fig. 16, whereas the temperature distributions in the undeformed meshes are presented in Fig. 17. For the aluminium sample, the differences are visible not only at the top corners of the sample but in the central part as well. Variant 1 gives horizontal isotherms in the reference configuration, which results in curved isotherms in the deformed mesh, compatible with the deformation of finite elements.

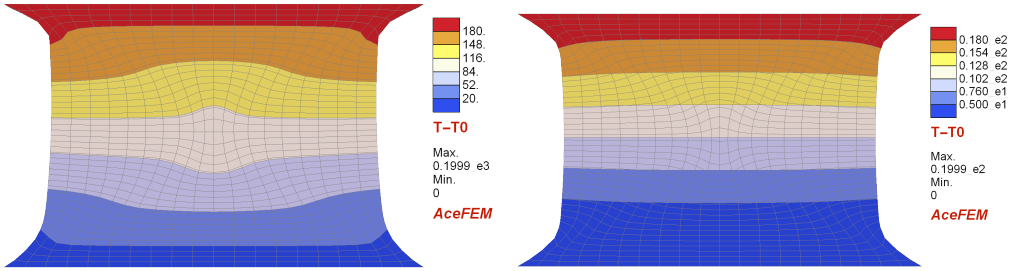

FIG. 16. Deformed mesh for the aluminium sample at the end of simulation with relative temperature distribution for variant 1 (left) and variant 2 (right) of Fourier's law.

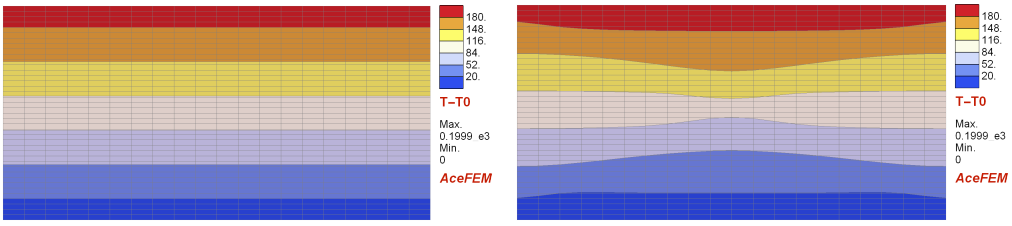

FIG. 17. Reference configuration of the aluminium sample with final relative temperature distribution for variant 1 (left) and variant 2 (right) of Fourier's law.

For the aluminium sample, the Cauchy heat flux density vectors are examined in one (top right) quarter of the specimen, see Fig. 18. It can be observed that despite the different temperature distributions the directions of the heat flow are very close for the two analysed variants. However, looking more closely at the most deformed part of the sample, it can be observed that the magnitudes of the heat flux vectors are different for the two variants. For variant 1, the heat flux vectors show a regular pattern even in the most deformed part of the sample, whereas the vectors for variant 2 have several times larger magnitude in the strongly deformed finite elements than in the remaining part of the sample. This behaviour is surprising and can be explained by the fact that variant 2 of Fourier's law is defined in the spatial configuration in which the finite element mesh evolves.

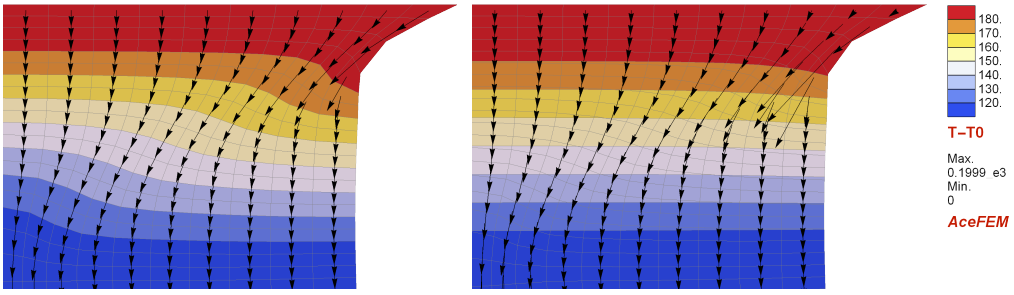

FIG. 18. Deformed mesh at the end of simulation for one-quarter of the aluminium sample with relative temperature distribution and Cauchy heat fluxes for variant 1 (left) and variant 2 (right) of Fourier's law.

For a deeper investigation of this issue, the most deformed part of the specimen is presented in Fig. 19 for the three analysed meshes. It can be seen that the finer the mesh is, the more distorted the elements are. The calculation of the spatial temperature gradient in a so strongly deformed mesh for variants 2 and 3

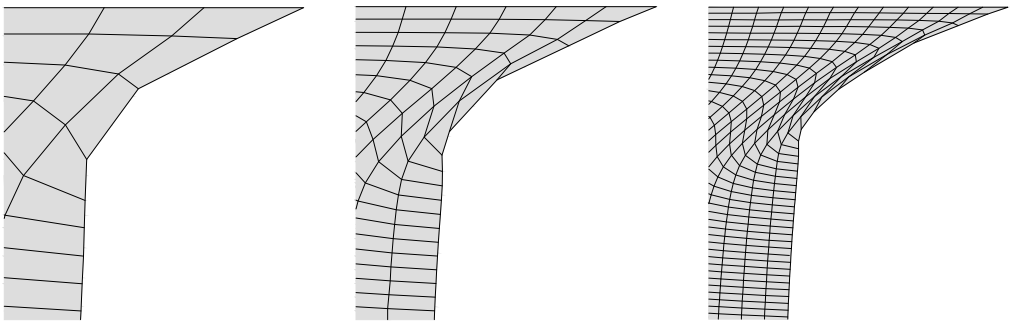

FIG. 19. Deformed meshes for the corner part of the aluminium sample at the end of simulation for three analysed meshes.

of Fourier's law is then unreliable. It can be concluded that for such large strains, the discretisation should be refined adaptively with growing deformation since this would provide a more reliable approximation of the temperature gradient calculated in the deformed configuration. The application of a finer mesh with a constant density (in the reference configuration) during the whole simulation does not help the problem and causes even greater local disturbances.

8. Conclusion

The aim of this paper was to contribute to a better understanding of different heat flux measures and isotropic forms of Fourier's law for a large-strain thermomechanical setting. For this purpose, a thorough analysis of common heat flux density vectors and the variants of Fourier's law specification has been performed. For a better interpretation, a simple analytical example has been calculated and discussed. It has been shown that by using Fourier's law in the current configuration for the Cauchy heat flux, the related Piola-Kirchhoff heat flux is not perpendicular to isotherms in the reference configuration and vice-versa.

For a more exhaustive analysis, computational tests have been performed via the FEM to investigate the influence of the adopted constitutive law for the heat flux on the results. Numerical simulations have revealed that the formulation of Fourier's law for a large-strain problem can influence the outcome related to a thermal field, for example, the sum of "reaction" heat fluxes at the surface with essential boundary conditions for temperature. Moreover, the distribution of temperature in the analysed specimen varied for the different Fourier's law variants, especially in the strongly deformed parts where temperature gradients were significant. The simulations of the rubber sample performed for changing process duration showed that a longer process allows for the transport of more heat towards the centre of the specimen, which resulted in more significant differences in temperature distribution and mechanical response for the analysed variants of Fourier's law. What is more, the application of Fourier's law in the reference configuration results in a more uniform temperature distribution in the sample. In the analysed cases, the local differences of temperature field slightly influence the global mechanical response. However, it should be emphasised that for a stronger thermomechanical coupling or high-temperature gradients in a strongly distorted sample the differences could be more significant.

It is interesting that for the different variants of Fourier's law resulting in the different temperature maps, the directions of the heat flow are close. Thus, the choice of Fourier's law does not significantly affect the general trajectory of the heat flux in the sample. However, in the most distorted finite elements, the Cauchy heat flux density vectors had much higher values for the spatial Fourier's law. The analysis presented in the paper leads to the impor-

tant observation that the calculation of a temperature gradient in the deformed configuration without adaptive mesh refinement can result in an unreliable approximation of the heat flux.

Taking into account all simulation results, it seems that the model which is closer to the physical behaviour is the one with the spatial Fourier's law formulation, where the spatial heat flux is directly proportional to the spatial temperature gradient, see Table 1. On the other hand, if the deformation-induced anisotropy is related not only to mechanical but also to thermal properties, then the application of the referential Fourier's law is reasonable. In such cases, the presence of a deformation gradient in the spatial heat flux reflects this fact and may be physically justified. However, from the computational viewpoint, the more efficient formulation is very often the material one, mainly due to less contribution to the tangent operator. Then, the application of Fourier's law for the Piola-Kirchhoff heat flux density vector, i.e., the referential heat flux directly proportional to the referential temperature gradient, seems to be a natural choice. In such a case, it should be clear that this can influence the thermal fields, in particular in the most distorted mesh parts of the simulated specimen.

References

1. Abeyaratne R., *Continuum Mechanics*, Volume II of Lecture Notes on the Mechanics of Solids, Electronic Publication, 2020, http://web.mit.edu/abeyaratne/lecture notes.html.

2. Abeyaratne R., Knowles J.K., On the stability of thermoelastic materials, *Journal of Elasticity*, **53**: 199–213, 1999, doi: 10.1023/A:1007513631783.

3. Bonet J., Wood R.D., *Nonlinear Continuum Mechanics for Finite Element Analysis*, 2nd ed., Cambridge University Press, Cambridge 2008.

4. Ĉanadija M., Brnić J., Associative coupled thermoplasticity at finite strain with temperature-dependent material parameters, *International Journal of Plasticity*, **20**(10): 1851–1874, 2004, doi: 10.1016/j.ijplas.2003.11.016.

5. de Souza Neto E.A., Perić D., Owen D.R.J., *Computational Methods for Plasticity. Theory and Applications*, John Wiley & Sons, Ltd, Chichester 2008.

6. Haupt P., *Continuum Mechanics and Theory of Materials*, Springer-Verlag, Berlin 2002.

7. Holzapfel G.A., Simo J.C., Entropy elasticity of isotropic rubber-like solids at finite strains, *Computer Methods in Applied Mechanics and Engineering*, **132**(1–2): 17–44, 1996, doi: 10.1016/0045-7825(96)01001-8.

8. Hughes T.J.R., *The Finite Element Method. Linear Static and Dynamic Analysis*, Prentice-Hall, New Jersey 1987.

9. Jemioło S., *Thermoelasticity and Heat Flux in Anisotropic Materials* [in Polish: *Termosprężystość i przepływ ciepła w materiałach anizotropowych*], Publishing House of the Warsaw University of Technology, Warsaw 2015.

10. Korelc J., Automation of the finite element method, [in:] *Nonlinear Finite Element Methods*, P. Wriggers [Ed.], Springer-Verlag, Berlin Heidelberg, 2008, pp. 483–508.

11. Korelc J., Automation of primal and sensitivity analysis of transient coupled problems, *Computational Mechanics*, **44**: 631–649, 2009, doi: 10.1007/s00466-009-0395-2.

12. Korelc J., Šolinc U., Wriggers P., An improved EAS brick element for finite deformation, *Computational Mechanics*, **46**: 641–659, 2010, doi: 10.1007/s00466-010-0506-0.

13. Korelc J., Wriggers P., *Automation of Finite Element Methods*, Springer, Switzerland 2016.

14. LeMonds J., Needleman A., Finite element analyses of shear localization in rate and temperature dependent solids, *Mechanics of Materials*, **5**(4): 339–361, 1986, doi: 10.1016/0167-6636(86)90039-6.

15. Miehe C., Entropic thermoelasticity at finite strains. Aspects of the formulation and numerical implementation, *Computer Methods in Applied Mechanics and Engineering*, **120**(3–4): 243–269, 1995, doi: 10.1016/0045-7825(94)00057-T.

16. Mucha M., Wcisło B., Pamin J., Simulation of PLC effect using regularized large-strain elasto-plasticity, *Materials*, **15**(12): Article no. 4327, 21 pages, 2022, doi: 10.3390/ma15124327.

17. Nowacki W., *Theory of Elasticity* [in Polish: *Teoria sprężystości*], PWN, Warsaw 1970.

18. Oppermann P., Denzer R., Menzel A., A thermo-viscoplasticity model for metals over wide temperature ranges-application to case hardening steel, *Computational Mechanics*, **69**(3): 541–563, 2021, doi: 10.1007/s00466-021-02103-4.

19. Reddy J.N., Gartling D.K., *The Finite Element Method in Heat Transfer and Fluid Dynamics*, CRC Press, Boca Raton 2010.

20. Ristinmaa M., Wallin M., Ottosen N.S., Thermodynamic format and heat generation of isotropic hardening plasticity, *Acta Mechanica*, **194**: 103–121, 2007, doi: 10.1007/s00707-007-0448-6.

21. Simo J.C., Numerical analysis and simulation of plasticity, [in:] *Handbook of Numerical Analysis*, P. Ciarlet, J. Lions [Eds], vol. VI, Elsevier Science B.V., Boca Raton, pp. 183–499, 1998.

22. Simo J.C., Miehe C., Associative coupled thermoplasticity at finite strains: Formulation, numerical analysis and implementation, *Computer Methods in Applied Mechanics and Engineering*, **98**(1): 41–104, 1992, doi: 10.1016/0045-7825(92)90170-O.

23. Vujošević L., Lubarda V.A., Finite-strain thermoelasticity based on multiplicative decomposition of deformation gradient, *Theoretical and Applied Mechanics*, **28–29**: 379–399, 2002, doi: 10.2298/TAM0229379V.

24. Wcisło B., Pamin J., Local and non-local thermomechanical modeling of elastic-plastic materials undergoing large strains, *International Journal for Numerical Methods in Engineering*, **109**(1): 102–124, 2017, doi: 10.1002/nme.5280.

25. Wriggers P., *Nonlinear Finite Element Methods*, Springer-Verlag, Berlin 2008.

26. Wriggers P., Miehe C., Kleiber M., Simo J.C., On the coupled thermomechnical treatment of necking problems via finite element methods, *International Journal for Numerical Methods in Engineering*, **33**(4): 869–883, 1992, doi: 10.1002/nme.1620330413.

27. Zienkiewicz O.C., Taylor R.L., Zhu J.Z., *The Finite Element Method: Its Basis and Fundamentals*, 6th ed., Elsevier Butterworth-Heinemann, 2005.

Received November 2, 2022; accepted version January 11, 2023.